

THE EFFECT OF PRECIPITATION CHARACTERISTICS ON HARDENING BEHAVIOR IN Cu–Cr–Sn ALLOY WITH Sn VARIATION

Zeyu Luo,¹ Fuxin Luo,¹ Weibin Xie,^{2,3}
Huiming Chen,² Hang Wang,² and Bin Yang^{1,2,3}

UDC 669.6:621.785

The influence of minor solute additions of Sn on hardening behavior and microstructure evolution of the Cu–Cr–Sn alloys has been investigated with help of an optical microscope, scanning electron microscope, transmission electron microscopy, and the Vickers hardness tester. Experimental results show that the Sn solutes, homogeneously distributed within the Cu matrix, provide a weak solid solution strengthening effect in the Cu–Cr–Sn alloy, nevertheless are important in enhancing precipitation hardening. The Cu–0.43Cr–0.36Sn alloy exhibits a significant age-hardening effect with a hardness increase by 62 HV after peak aging at 450°C, which is stronger than that of the Cu–0.43Cr–0.08Sn and the Cu–0.43Cr–0.17Zr–0.05Mg–0.1RE alloys. A trace amount of Sn is highly effective at suppressing the transformation of the Cr-rich phase from the face-centered cubic (FCC) into the body-centered cubic (BCC) structure in the Cu–Cr alloys during the aging process, and therefore the FCC Cr-rich precipitate is the dominant strengthening phase in the Cu–Cr–Sn alloys. Besides, a higher areal number density of Cr-rich precipitates ($\sim 4.2 \cdot 10^{15} \text{ m}^{-2}$) was observed in peak-aging Cu–0.43Cr–0.36Sn alloy as compared to Cu–0.43Cr–0.08Sn alloy, which shows that the adding Sn to Cu–Cr alloy can accelerate the nucleation of the Cr-rich precipitates. The improvement of precipitation hardening and hardening kinetics in the Cu–0.43Cr–0.36Sn alloy is mainly attributed to the acceleration in the nucleation of Cr-rich precipitates through Sn addition.

Keywords: Cu–Cr–Sn alloy, Sn element, hardening, aging, microstructure.

INTRODUCTION

Precipitation-hardenable Cu–Cr alloys have a great potential to be applied in aerospace, rail transportation, and electrical engineering due to their excellent combination of strength, electrical and thermal conductivity [1–3]. Significant improvement in strength and hardness (compared to pure copper) is caused by precipitation of the nanoscale Cr-rich particles in the Cu–Cr alloys [4], which are identified as an intermetallic compound consisting of Cu and Cr by atom probe tomography (APT) [3, 5]. According to the equilibrium phase diagram of the Cu–Cr system [6], solid solubility of Cr in Cu is low (below 0.03 at.%) at temperatures below 500°C. Thus, high

¹School of Materials Science and Engineering, Jiangxi University of Science and Technology, Ganzhou 341000, PR China. ²Institute of Engineering Research, Jiangxi University of Science and Technology, Ganzhou 341000, PR China.

³To whom correspondence should be addressed; e-mail: x881109100@163.com, yangbin65@126.com.

Published in Poroshkova Metallurgiya, Vol. 58, Nos. 11–12 (530), pp. 45–56, 2019. Original article submitted May 23, 2019.

conductivity in the Cu–Cr alloys is achieved after aging treatment due to the low content of Cr solute in the Cu matrix solid solution [7].

The precipitation sequence of binary Cu–Cr and ternary Cu–Cr–Zr alloys can be described as following: supersaturated Cu solid solution → FCC; Cr-rich phase → BCC; Cr-rich phase [8, 9]. Metastable Cr-rich cluster with FCC structure forms in the initial stage of aging and gradually transforms into BCC structure with prolongation of aging time [9]. However, it is found that alloying elements significantly affect the FCC → BCC transformation. Wang et al [10] have reported that Ti addition can hinder the nucleation of equilibrium BCC Cr-rich precipitates, which suppresses the FCC → BCC transformation of the Cr-rich phase in the Cu–Cr–Zr–Ti alloy. Therefore, the dominant precipitates of the Cu–Cr–Zr–Ti alloy retain FCC structure even at the over-aged stage.

Numerous modified Cu–Cr alloys with higher strength and electrical conductivity have been developed, namely Cu–Cr–Ag [11] and Cu–Cr–Zr alloys [12]. It is reported that the addition of the alloying elements plays a significant role in improving the comprehensive properties of the Cu–Cr alloys [13, 14]. Its influence of on the mechanical properties in the Cu–Cr alloys is mainly associated with the following three aspects. Firstly, the alloying elements in the Cu–Cr alloy induce the formation of a new strengthening precipitate. In the Cu–0.75Cr–0.1Zr alloy, two strengthening phases (Cr phase and Cu₄Zr phase) precipitates in the matrix, which leads to a significant increase in precipitation strengthening effect (compared to Cu–Cr binary alloy) [15]. Secondly, the alloying elements can enhance solid solution strengthening effect due to the increase of lattice parameter misfit with the matrix. Islamgaliev discovered that addition of 0.1% Ag increased tensile strength (up to ~50 MPa) through solid solution strengthening [16]. Thirdly, the alloying elements can influence the precipitate characteristics of the Cr-rich phase, such as precipitate size, distribution, and structure. For example, Mg can promote the precipitate nucleation and inhibit the precipitate growth in the Cu–Cr–Mg alloy, and thereby improve the strength and softening resistance of the alloy [3].

Sn element addition has been widely used in Cu–Cr alloys to prepare lead frame materials such as C18020, C18141 [17]. Ide [18] believed that the trace addition of Sn in Cu can enhance solid solution strengthening effect and increase the strength of pure copper. However, the effect of Sn element on the microstructure and mechanical properties of Cu–Cr alloys are reported rarely. In this work, we investigated the precipitation hardening behavior and microstructure evolution of Cu–Cr–Sn alloys during isothermal aging at 450°C and provided the interrelationships between Sn content, microstructure, and hardness. Detailed information about structural and chemical composition helps to clarify the strengthening effects of Sn addition and thereby provides useful hints to develop high-performing Cu–Cr alloys.

MATERIALS AND EXPERIMENTAL PROCEDURE

The Cu–Cr–Sn alloys were melted in a medium frequency induction furnace (DS-7-003, Wuxi Doushan Furnace) with adding cathode copper (99.95 wt.%), pure tin (99.99 wt.%), and Cu–8 wt.% Cr intermediate alloy. The melt was cast into an iron mold followed by air cooling to room temperature, and an alloy ingot with a size of 120 mm × 80 mm × 20 mm was obtained. A quantitative estimate of the composition of the alloy ingots was carried out by an inductively coupled plasma emission spectroscopy (ICP, IRIS Intrepid II, Thermo Fisher Scientific). Obtained results are shown in Table 1. The solution heat treatment is usually an important stage to dissolve the second intermetallic phase into the matrix [19]. The as-cast alloys were solution heat-treated at 900°C for 60 min in an electrical resistance furnace (SX2-10-13, Shanghai Shiyan), followed by rapid water quenching. Subsequently, the solution-treated materials were cut into samples of 20 mm × 20 mm × 3 mm and then subjected to isothermal aging treatment at 450°C.

TABLE 1. Chemical Compositions of the Cu–Cr–Sn Alloys (wt.%)

Alloy	Cr	Sn	O	S	P	Cu
1	0.43	0.36	0.002	0.002	0.001	Bal.
2	0.43	0.08	0.002	0.001	0.001	Bal.

Hardness measurements of the alloy were carried out using a Vickers hardness tester (200HVS-5, Laizhou Huayin) with a load of 0.2 kg and a loading time of 10 sec.

The microstructures of the Cu–Cr–Sn alloys were characterized by optical microscopy (BMM-90AE, Shanghai Bimu), scanning electron microscopy (SEM, MIRA3 LMH, TESCAN-ORSAY HOLDING a.s.), and transmission electron microscopy (TEM, Tecnai-G2-F20, FEI). The samples for SEM investigation were first mechanically grounded and then electrolytically polished in an electrolyte of 8 vol.% perchloric acid in ethanol at –30 °C. Subsequently, the selected samples were examined by SEM, equipped with an energy disperse spectrometer (EDS, 9806A-1UPS-SN, Thermo Fisher Scientific). The samples for TEM investigation were mechanically grounded to ~50 μm in thickness and then thinned by twin-jet electropolishing using an electrolyte of 25 vol.% nitric acid in methanol at –35°C.

RESULTS

Hardness Behavior of Cu–Cr–Sn Alloys. The hardness of the as-cast and solution-treated Cu–Cr–Sn alloy is shown in Fig. 1. It can be seen that the hardness of the as-cast Cu–0.43Cr–0.36Sn alloy (denoted as high Sn alloy) is ~108 HV, which is slightly higher than that of the Cu–0.43Cr–0.08Sn alloy (93 HV). After solution heat treatment at 900°C, the hardness of the Cu–0.43Cr–0.36Sn and Cu–0.43Cr–0.08Sn alloys decreased to 69 HV and 67 HV, respectively. Only a small difference in hardness is observed between the two solution-treated alloys.

Figure 2 shows the hardness evolution of Cu–0.43Cr–0.36Sn and Cu–0.43Cr–0.08Sn alloys during aging at 450°C. A significant age hardening is observed in both alloys. The hardness of the Cu–Cr–Sn alloys increases rapidly at the beginning of aging, and reach the peak after aging for 2 h. The Cu–0.43Cr–0.36Sn alloy exhibited a higher peak hardness (~130 HV) compared to the Cu–0.43Cr–0.08Sn alloy. The peak hardness of the Cu–0.43Cr–0.36Sn alloy is by ~15 HV higher than that of the Cu–0.43Cr–0.08Sn alloy. During further aging, the hardness of the alloys slightly decreases (over aging). In Cu–0.43Cr–0.36Sn alloy, the hardness gradually decreases to 120 HV after aging for 12 h.

Microstructures. The microstructures of the as-cast Cu–Cr–Sn alloys are shown in Fig. 3, the coarse grains with a size of more than 600 μm are observed in Figs. 3a and 3b. No significant difference in grain size between Cu–0.43Cr–0.36Sn and Cu–0.43Cr–0.08Sn alloys are observed. In addition, a large number of black particles are detected in the interior of the grains. The morphology of the black particles, determined by SEM observation, is dendritic (Figs. 3c and 3d). Compared to Cu–0.43Cr–0.08Sn alloy, the second-phase particles of the Cu–0.43Cr–0.36Sn alloy are finer and more dispersed.

EDS analysis on the second-phase particles of the as-cast Cu–0.43Cr–0.36Sn alloy is shown in Fig. 4. The EDS results show that the Cr element is present inside the second-phase particles in significantly higher concentration than in the matrix, which indicates that the second-phase particle should be the Cr phase. A large amount of undissolved Cr phase particles is formed in the interior of the grains during casting. Besides, the Sn element is uniformly distributed in the matrix.

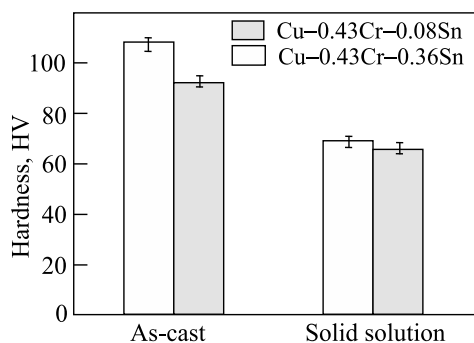


Fig. 1. Hardness of the as-cast and solution treated Cu–Cr–Sn alloy

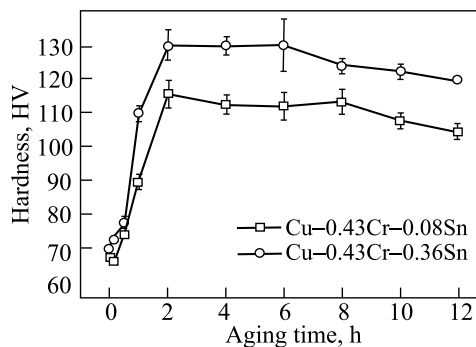


Fig. 2. Hardness variations of the Cu–Cr–Sn alloys during 450°C isothermal ageing

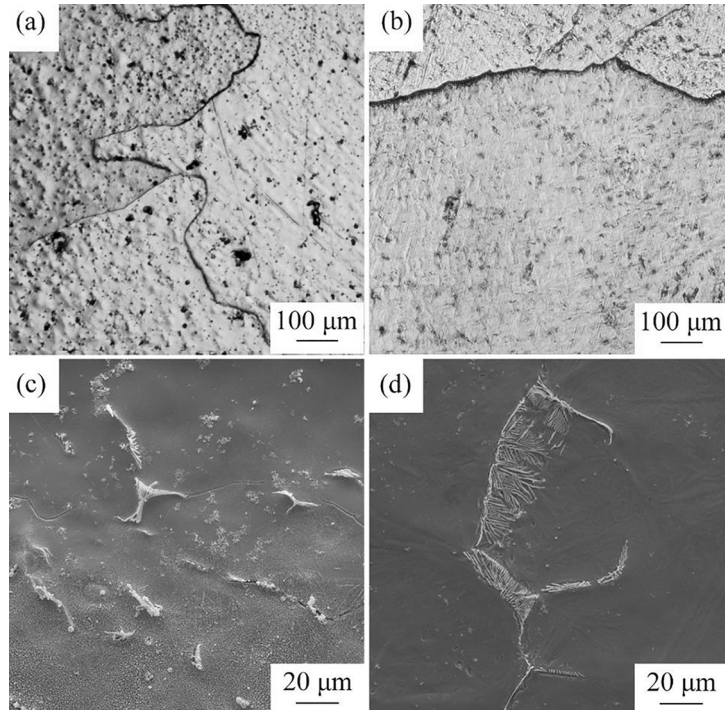


Fig. 3. OM (a, b) and SEM (c, d) images of the as-cast (a, c) Cu-0.43Cr-0.36Sn and (b, d) Cu-0.43Cr-0.08Sn alloys

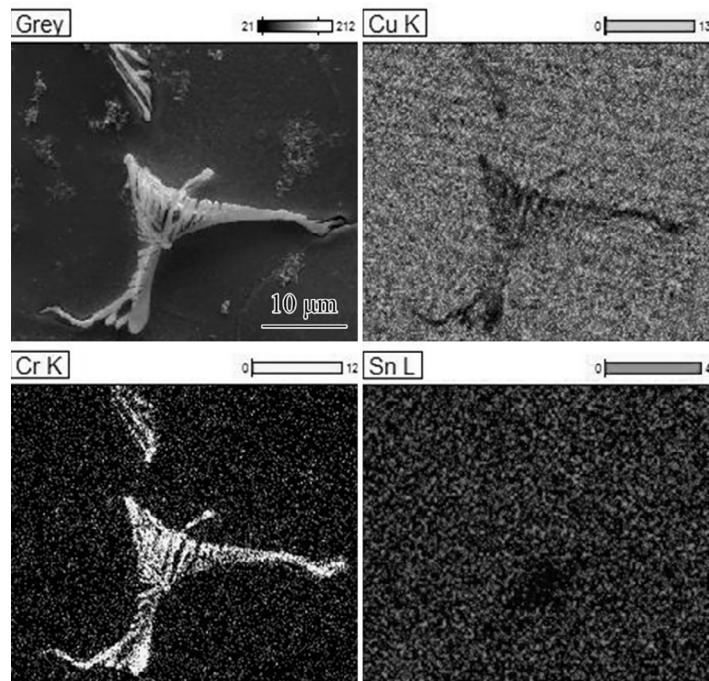


Fig. 4. SEM image and EDS element dot-maps of the as-cast Cu-0.43Cr-0.36Sn alloy

Figure 5 depicts the TEM bright-field images of the as-cast Cu-Cr-Sn alloys. It can be seen that a large number of nanometer-scale second-phase particles are dispersed in the matrix. Figure 5a shows the presence of spherical precipitates, that are uniformly distributed throughout the matrix grains with a diameter of ~ 4 nm. This indicates that nanoscale particles are precipitated during slow cooling with following casting. The as-cast Cu-0.43Cr-0.36Sn alloy exhibits a higher volume fraction of the nanoscale particles versus the Cu-0.43Cr-0.08Sn alloy.

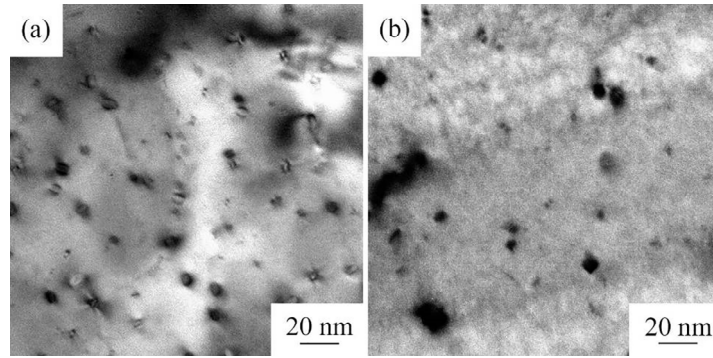


Fig. 5. Bright-field TEM micrographs of the as-cast (a) Cu-0.43Cr-0.36Sn and (b) Cu-0.43Cr-0.08Sn alloys

The coarse grains larger than 600 μm in diameter are detected in the solution-treated Cu-Cr-Sn alloys as shown in Fig. 6, and there are no significant changes in grain characterization compared to the as-cast alloys. Besides, the volume fraction of Cr phases in the grains significantly reduced after solution heat treatment (Figs. 6*b* and 6*c*), which indicates that the majority of the Cr phase particles are dissolved into the copper matrix during solution heat treatment at 950°C.

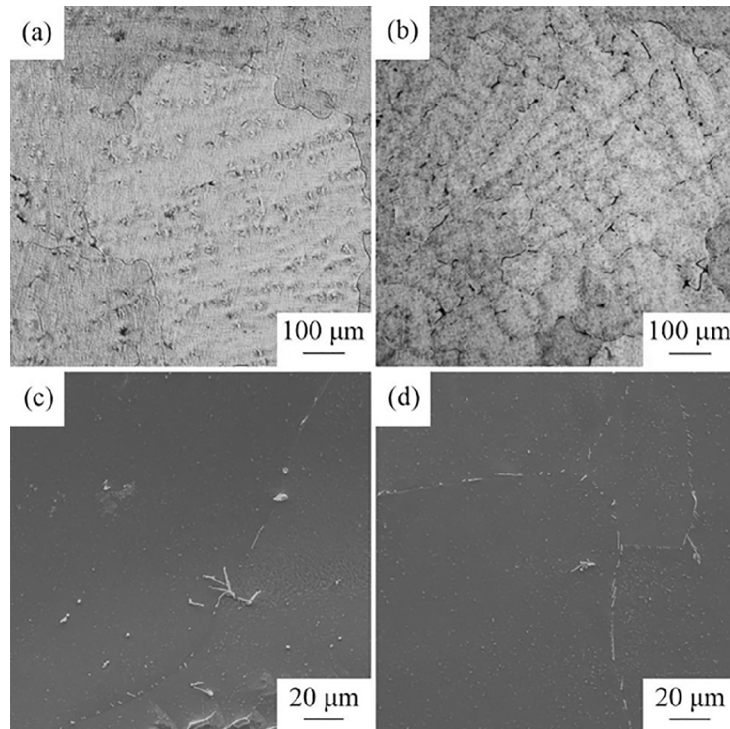


Fig. 6. OM (a, b) and SEM (c, d) images of solution-treated (a, c) Cu-0.43Cr-0.36Sn and (b, d) Cu-0.43Cr-0.08Sn alloys

Figure 7 shows the microstructures of the solution-treated Cu-0.43Cr-0.36Sn and Cu-0.43Cr-0.08Sn alloys. Only a few dislocations are observed in the matrix, and the dispersed nanoscale second phase particles have completely dissolved in the matrix during the solution heat treatment.

Figure 8 shows TEM images and corresponding selected area electron diffraction (SAED) patterns of precipitates within the Cu matrix in Cu-0.43Cr-0.36Sn alloy aged at 450°C. The granulate-like precipitates of an average diameter ~ 5 nm are formed in the matrix uniformly during the early stage of aging (Fig. 8*a*). A precipitate

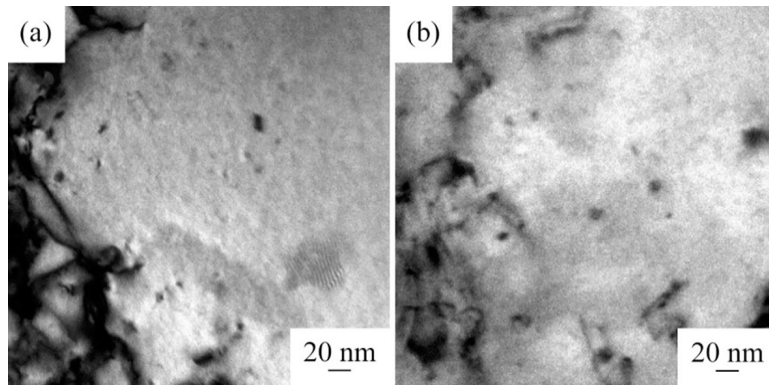


Fig. 7. Bright-field TEM images of solution-treated (a) Cu-0.43Cr-0.36Sn and (b) Cu-0.43Cr-0.08Sn alloys

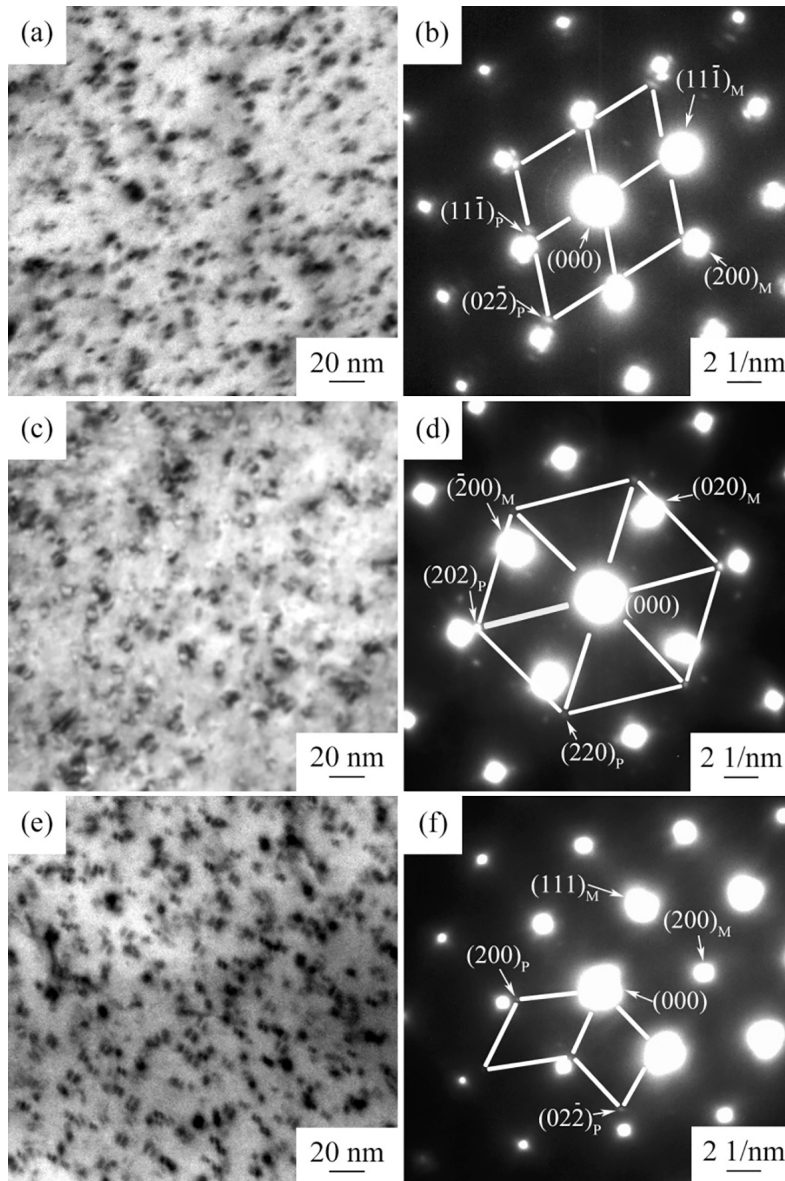


Fig. 8. Bright-field TEM and selected area electron diffraction images of Cu-0.43Cr-0.36Sn alloy after aging treatment: a, b) 450°C for 1 h; c, d) 450°C for 2 h; e, f) 450°C for 8 h

areal number density of $4.2 \cdot 10^{15} \text{ m}^{-2}$ is measured in the under-aged sample. As shown in Fig. 8b, the crystallographic structure of precipitate is identified as a face-centered cubic structure by selected-area electron diffraction (SAED) pattern. The precipitates with FCC structure are determined to metastable Cr-rich phase by APT in the Cu–Cr alloys [5, 11]. Cr-rich precipitates are aligned along the $[022]_M$ (M: Matrix) directions and are semi-coherent with the Cu matrix (the lattice parameter misfit is $\sim 14\%$). The orientation relationship between Cr-rich phase and the Cu matrix is $(200)_M // (200)_P$, $[011]_M // [011]_P$.

With the further extension of the aging times, precipitates size and precipitate areal number density remains nearly unchanged in the Cu–Cr–Sn alloy (Figs. 8c and 8e). The precipitates still exhibit an FCC structure (Fig. 8f) even after long aging time (8 h) at 450°C . The lattice parameter of the precipitates is calculated to be $\sim 0.404 \text{ nm}$ in the Cu–0.43Cr–0.36Sn alloy. In addition, a different orientation relationship between the Cr-rich precipitate and the matrix ($(220)_M // (220)_P$, $[111]_M // [001]_P$) is observed in the aged Cu–Cr–Sn alloys (Fig. 8d). The lattice parameter misfit between precipitate and matrix along $(200)_P // (111)_M$ direction is $\sim 0.3\%$, and thereby Cr-rich precipitate is coherent with a matrix.

TEM images and corresponding selected area electron diffraction (SAED) patterns of precipitates within the Cu matrix in Cu–0.43Cr–0.08Sn alloy aged at 450°C are shown in Fig. 9. The FCC Cr-rich precipitates with an average diameter of $\sim 7 \text{ nm}$ are detected in the matrix of the Cu–0.43Cr–0.08Sn alloy aged for 1 h (Figs. 9a and 9b).

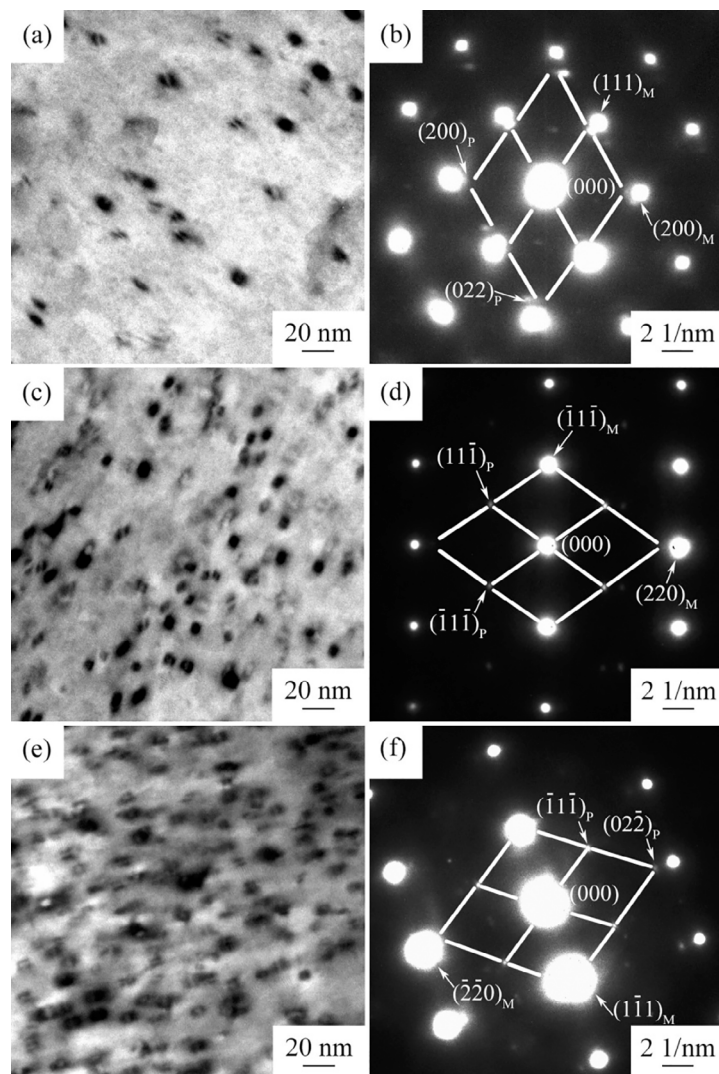


Fig. 9. Bright-field TEM and selected area electron diffraction images of Cu–0.43Cr–0.08Sn alloy after aging treatment: a, b) 450°C for 1 h; c, d) 450°C for 2 h; e, f) 450°C for 8 h

It reveals qualitatively that the number density of the Cr-rich precipitates at the under-aged stages of Cu–0.43Cr–0.08Sn alloy is $\sim 0.6 \cdot 10^{15} \text{ m}^{-2}$, which is much lower than in Cu–0.43Cr–0.36Sn alloy. The amount of the Cr-rich precipitates increases significantly with prolonging aging time (Figs. 9c and 9e), and the number density of the precipitates increases to $2.1 \cdot 10^{15} \text{ m}^{-2}$ in the Cu–0.43Cr–0.08Sn alloy aged for 8 h. At the over-aged stages, only FCC Cr-rich precipitates are detected within the grains. Similarly, to Cu–0.43Cr–0.36Sn alloy, two orientation relationships between the Cr-rich phase and Cu matrix are observed in the Cu–0.43Cr–0.08Sn alloy (Figs. 9b, 9d, and 9f). In addition, the lattice parameter of the precipitates is calculated to be $\sim 0.399 \text{ nm}$ in the Cu–0.43Cr–0.08Sn alloy.

DISCUSSION

Results presented in Figs. 1 and 2 show that the Cu–0.43Cr–0.36Sn alloy exhibits a higher as-cast and peak aging hardness ($\sim 15 \text{ HV}$ higher) compared to the Cu–0.43Cr–0.08Sn alloy. It is demonstrated that the addition of Sn improves the hardness of the Cu–Cr–Sn alloys. Based on the Cu–Sn binary phase diagram [20], the added Sn element can be completely dissolved in the Cu matrix of both alloys due to relatively high solubility limit of Sn in Cu (more than 8 wt.% at 450°C). EDS measurement (Fig. 4) indicates that Sn is fairly uniformly distributed within the Cu matrix of the Cu–Cr–Sn alloys. However, the hardness of the solid-solution treated Cu–0.43Cr–0.36Sn alloy is 2 HV higher than that of the Cu–0.43Cr–0.08Sn alloy, which reveals that the solid-solution strengthening produced by the Sn solute-atoms provides only a small contribution to the total hardness in the Cu–0.43Cr–0.36Sn alloy.

Microstructure observations (Figs. 3 and 6) show that the finer grains and Cr particles are detected in the as-cast Cu–0.43Cr–0.36Sn alloy as compared to Cu–0.43Cr–0.08Sn alloy, while both of two alloys exhibit coarse grains ($>500 \mu\text{m}$) and micron-size Cr phase particles. Their effect on mechanical properties is established to be very small [15]. Therefore, the contribution of coarse grain and micron-size Cr phase particles to the hardness in the Cu–Cr–Sn alloys can be neglected here. Besides, the difference in precipitation characteristics (such as size and number density of precipitates) between Cu–0.43Cr–0.36Sn and Cu–0.43Cr–0.08Sn alloy is significant (Figs. 5, 8, and 9), which indicates that small variations in the Sn content can lead to sensitive differences in the precipitation behaviors. It is known that precipitation strengthening effect depends on the precipitate characteristics [2]. The improvement of hardness in Cu–Cr–Sn alloys should be mainly attributed to the influence of Sn on precipitation behavior. For comparison, the increment hardness of the Cu–0.43Cr–0.08Sn and the Cu–0.43Cr–0.17Zr–0.05Mg–0.1RE [21] alloy after peak aging at 450°C is 47 and 53 HV, respectively, which is lower than that of Cu–0.43Cr–0.36Sn alloy (62 HV). The addition of Sn (more than 0.36 wt.%) can significantly improve the total hardness through influencing the precipitation hardening behavior of Cu–Cr alloys.

The structural transformation of the FCC precipitate toward the BCC structure occurs in binary Cu–Cr alloys [8] and ternary Cu–Cr–Zr alloys [5], and the precipitates with a BCC structure can be found in the peak-aged samples. However, it is apparent from Figs. 8 and 9 that only Cr-rich precipitates with FCC structure found in the Cu–Cr–Sn alloys during the aging process. Even at the over-aged stages, no BCC precipitates are detected in both alloys. It is indicated that small additions of Sn can suppress the FCC \rightarrow BCC phase transformation in Cu–Cr alloys. Therefore, the nanoscale Cr-rich phase with FCC structure is the dominant strengthening phase in the Cu–Cr–Sn alloy, and the improvement in hardness of the Cu–Cr–Sn alloys at peak aging stage is mainly attributed to the precipitation of FCC Cr-rich phase.

The precipitation hardening effect depends on the interactions between mobile dislocations and precipitates. According to the investigation on precipitation strengthening mechanism, the peak hardness of age-hardening alloy usually corresponds to a transition from a shearing mechanism to a dislocation bypassing mechanism [22]. Based on the Orowan strengthening models [23], the precipitation hardening effect can be improved by decreasing the inter-nanoprecipitate distance. The Cu–0.43Cr–0.36Sn alloy exhibits a higher areal number density of Cr-rich precipitates with smaller radii during the aging process compared to Cu–0.43Cr–0.08Sn alloy. It is implied that Sn adding can increase the number density of Cr-rich precipitates in peak-aged Cu–Cr alloys, which leads to a smaller mean distance between the Cr-rich precipitates in peak-aged Cu–0.43Cr–0.36Sn

alloy. Thereby, the peak-aged Cu–0.43Cr–0.36Sn alloy exhibits a hardness increment (62 HV) higher than that of Cu–0.43Cr–0.08Sn alloy (47 HV).

The improvement of the age-hardening effect in high Sn alloy is mainly attributed to the increase in precipitation nucleation by Sn adding. The areal number density for FCC Cr-rich precipitates in the Cu–0.43Cr–0.36Sn alloy is approximately seven times higher than that of Cu–0.43Cr–0.08Sn alloy (~ 4.2 vs. $0.6 \cdot 10^{15} \text{ m}^{-2}$) at the under-aged stages (aged for 1 h). It is indicated that the addition of Sn to the Cu–Cr alloy accelerates the process of precipitation nucleation. A system with a high density of nuclei is beneficial for accelerated precipitation kinetic due to small diffusion distance to be covered by solutes [24]. Therefore, the addition of Sn to the Cu–Cr alloy has induced a higher areal number density of Cr-rich precipitates in the high Sn alloy after peak aging, producing a higher level of precipitation strengthening than that of the low Sn alloy. Furthermore, compared to Cu–0.43Cr–0.08Sn alloy, a faster rate of age hardening is observed in Cu–0.43Cr–0.36Sn alloy, further suggesting that Sn can also enhance precipitation kinetics in Cu–Cr alloys.

CONCLUSIONS

The relationship between Sn content, microstructure and hardening behavior of Cu–Cr–Sn alloys were investigated in this paper. The effect of Sn micro-alloying additions on the precipitation hardening behavior of the Cu–Cr alloys have been determined. Based on our experimental results, the following conclusions can be drawn.

The solid-solution strengthening effect produced by a trace amount of Sn solute-atoms provides only a small contribution to the total hardness of the Cu–Cr–Sn alloy. The improvement in total hardness of the high Sn alloy is mainly attributed to the influence of Sn on precipitation strengthening.

Additions of Sn can suppress the FCC \rightarrow BCC phase transformation in the Cu–Cr alloy, and the age precipitation hardening behavior of the Cu–Cr–Sn alloys is mainly contributed to nanoscale Cr-rich precipitates with FCC structure.

Sn addition to the Cu–Cr alloy accelerates the precipitation nucleation, which results in higher precipitate number density, and thereby improves the precipitation hardening effect and hardening kinetics in high Sn-containing alloy.

REFERENCES

1. Gencaga Purcek, Hilmi Yanar, Onur Saray, Ibrahim Karaman, and Hans Jürgen Maier, “Effect of precipitation on mechanical and wear properties of ultrafine-grained Cu–Cr–Zr alloy,” *Wear*, **311**, No. 1–2, 149–158 (2014).
2. S. Chenna Krishna, G. Sudarsana Rao, Abhay K. Jha, Bhanu Pant, and P.V. Venkitakrishnan, “Strengthening in high strength Cu–Cr–Zr–Ti alloy plates produced by hot rolling,” *Mater. Sci. Eng. A.*, **674**, 164–170 (2016).
3. Ziqian Zhao, Zhu Xiao, Zhou Li, Muzhi Ma, and Jie Dai, “Effect of magnesium on microstructure and properties of Cu–Cr alloy,” *J. Alloy. Compd.*, **752**, 191–197 (2018).
4. A. Morozova and R. Kaibyshev, “Grain refinement and strengthening of a Cu–0.1Cr–0.06Zr alloy subjected to equal channel angular pressing,” *Philos. Mag.*, **97**, No. 24, 2053–2076 (2017).
5. A. Chbihi, X. Sauvage, and D. Blavette, “Atomic scale investigation of Cr precipitation in copper,” *Acta Mater.*, **60**, No. 11, 4575–4585 (2012).
6. M.A. Turchanin, “Phase equilibria and thermodynamics of binary copper systems with 3d-metals. III. Copper-Chromium system,” *Powder Metall. Met. Ceram.*, **45**, No. 9–10, 457–467 2006. Vol..
7. R. Mahmudi, A. Karsaz, A. Akbari-Fakhrabadi, and Geranmayeh Abdolreza, “Impression creep study of a Cu–0.3Cr–0.1Ag alloy,” *Mater. Sci. Eng. A.*, **527**, No. 10–11, 2702–2708 (2010).
8. Lijun Peng, Haofeng Xie, Guojie Huang, Gaolei Xu, Xiangqian Yin, XueFeng, Xujun Mi, and Zhen Yang, “The phase transformation and strengthening of a Cu–0.71 wt.% Cr alloy,” *J. Alloys Compd.*, **708**, 1096–1102 (2017).

9. Chen Xiaobo, Jiang Feng, Lele Liu, Hongfeng Huang, and Zhangzhi Shi, "Structure and orientation relationship of new precipitates in a Cu–Cr–Zr alloy," *Mater. Sci. Tech.*, **34**, No. 3, 282–288 (2018).
10. Hang Wang, Liukui Gong, Jinfa Liao, Huiming Chen, Weibin Xie, and Bin Yang, "Retaining meta-stable fcc-Cr phase by restraining nucleation of equilibrium bcc-Cr phase in CuCrZrTi alloys during ageing," *J. Alloys Compd.*, **749**, 140–145 (2018).
11. C. Watanabe, R. Monzen, and K. Tazaki, "Mechanical properties of Cu–Cr system alloys with and without Zr and Ag," *J. Mater. Sci.* **43**, No. 3, 813–819 (2008).
12. S. Viorica, "Influence of thermomechanical treatment on microstructure and properties of electroslag remelted Cu–Cr–Zr alloy," *Mater. Design.*, **51**, No. 10, P. 688–694 (2013).
13. Pengchao Zhang, Jinchuan Jie, Yuan Gao, Hang Li, Tongmin Wang, and Tingju Li, "Influence of cold deformation and Ti element on the microstructure and properties of Cu–Cr system alloys," *J. Mater. Res.* 2015. Vol. 30, No. 13. P. 2073–2080.
14. Y. Pang, C.D. Xia, M.P. Wang, et al., "Effects of Zr and (Ni, Si) additions on properties and microstructure of Cu–Cr alloy," *J. Alloys Compd.*, **582**, No. 5, 786–792 (2014).
15. U. Holzwarth, H. Stamm, "The precipitation behaviour of ITER-grade Cu–Cr–Zr alloy after simulating the thermal cycle of hot isostatic pressing," *J. Nucl. Mater.*, **279**, No. 1, 31–45 (2000).
16. R.K. Islamgaliev, K.M. Nesterov, J. Bourgon., et al., "Nanostructured Cu–Cr alloy with high strength and electrical conductivity," *J. Appl. Phys.*, **115**, No. 19, 1943011–1943014 (2014).
17. J.H. Su, P. Liu, Q.M. Dong, et al., "Aging study of rapidly solidified and solid-solution Cu–Cr–Sn–Zn alloy," *J. Mater. Process. Tech.*, **205**, No. 1–3, 366–369 (2008).
18. N. Ide, K. Hayakawa, and S. Asano, "Evaluation of microplastic flow stress in copper alloys from amplitude-dependent internal friction," *Mater. Trans.*, **42**, No. 3, 435–438 (2015).
19. B. Lin, W. Zhang, Y. Zhao, and Y. Li, "Solid-state transformation of Fe-rich intermetallic phases in Al–5.0Cu–0.6Mn squeeze cast alloy with variable Fe contents during solution heat treatment," *Mater. Charact.*, **104**, 124–134 (2013).
20. S. Fürtauer, D. Li, D. Cupid, H. Flandorfer, "The Cu–Sn phase diagram. Part I: New experimental results. *Intermetallics*," **34**, 142–147 (2013).
21. S.G. Mu, Y.Q. Tang, F.A. Guo, X.M. Cao, "Study on microstructure and properties of aged Cu–Cr–Zr–Mg–RE alloy," *Mater. Sci. Eng. A.*, **475**, No. 1–2, 235–240 (2008).
22. X.F. Huang, W.Z. Zhang, "Improved age-hardening behavior of Mg–Sn–Mn alloy by addition of Ag and Zn," *Mater. Sci. Eng. A.*, **552**, 211–221 (2012).
23. A.D. Luca, D.C. Dunand, and D.N. Seidman, "Microstructure and mechanical properties of a precipitation-strengthened Al–Zr–Sc–Er–Si alloy with a very small Sc content," *Acta Mater.*, **144**, 80–91 (2018).
24. E. Gumbmann, F. De Geuser, and Ch. Sigli, "Influence of Mg, Ag and Zn minor solute additions on the precipitation kinetics and strengthening of an Al–Cu–Li alloy," *Acta Mater.*, **133**, 172–185 (2017).